Available online at www.sciencedirect.com
ScienceDirect
Journal of Power Sources 174 (2007) 927–931
JOURNAL OF POWER SOURCES
www.elsevier.com/locate/jpowsour

Short communication

The effect of Al substitution on the lithium insertion properties of lithium vanadium fluorophosphate, $LiVPO_4F$

J. Barker *, M.Y. Saidi, R.K.B. Gover, P. Burns, A. Bryan

Valence Technology Inc., 1889 East Maule Avenue, Suite A, Las Vegas, NV 89119, USA

Available online 23 June 2007

Abstract

The structural and electrochemical insertion properties of $LiV_{1-x}Al_xPO_4F$ ($x = 0.00$, 0.25 and 0.50) phases are presented. XRD data reveal that the basic triclinic amblygonite structure was retained for all experimental compositions. Although the material specific capacities decreased almost linearly with aluminum content, the substituted phases revealed some intriguing properties that appear to be 'tunable' within the compositional range under investigation. The main beneficial attributes include low voltage polarization, high operating voltage and comparatively low capacity fade on cycling. In all cases the observed lithium insertion behavior was restricted to the $V^{3+/4+}$ redox couple.

Keywords: Lithium-ion; Vanadium; Fluorophosphate; Aluminum substitution; Batteries

1. Introduction

Framework materials based on the phosphate polyanion building block are being increasingly regarded as favorable replacements for conventional oxide-based materials as positive electrodes in lithium-ion battery applications. The lithium insertion phases $LiFePO_4$ [1] and $Li_3V_2(PO_4)_3$ [2] were the first of such materials to be identified and characterized. Recently, in an extension of this basic approach, our group has described the insertion properties of lithium vanadium fluorophosphate, $LiVPO_4F$ [3–7]. X-ray powder diffraction studies indicate that the $LiVPO_4F$ is *iso*-structural with the naturally occurring minerals tavorite, $LiFePO_4OH$ [8] and amblygonite, $LiAlPO_4F$ [9], crystallizing with a triclinic structure (space group *P*-1). The $LiVPO_4F$ structure comprises a three-dimensional framework built up from $[PO_4]$ tetrahedra and $[VO_4F_2]$ octahedra [6,7] wherein the oxygen atoms are shared between the two environments. The strong inductive effect of the PO_4^{3-} anion, combined with the presence of structural fluorine, moderates the energetics of the transition-metal redox couple such that the reversible lithium insertion reactions for $Li_{1-x}VPO_4F$ operate at around 4.2 V versus lithium. This unusually high operating potential allows the fluorophosphate phase to be employed as the positive electrode in high energy density graphite-based lithium-ion cells [6,7].

Following the successful preparation and optimization of the parent $LiVPO_4F$ material, we have turned our attention to modifying the structure and electrochemical properties using a range of substitutional strategies. One of the more promising of these approaches has been the replacement of V^{3+} with Al^{3+}, since the ionic radii of these ions within a sixfold coordination environment are similar. Moreover, since $LiVPO_4F$ is *iso*-structural with the mineral amblygonite ($LiAlPO_4F$), the aluminum-substituted compositions were considered likely to exist as single structural phases. Although the substituted aluminum will be electrochemically inactive, it was considered that its incorporation might facilitate some other beneficial properties. For instance, the presence of the Al might be used to "fine tune" the operational performance. For example, the possible accessing of the V^{4+}/V^{5+} redox couple and the lower atomic mass of the aluminum (compared to vanadium), may allow the preparation of active phases with both enhanced specific capacities and higher operating voltages.

2. Experimental

The $LiV_{1-x}Al_xPO_4F$ phases used in this study were prepared by a two-step carbothermal reduction (CTR) method [10,11]. The substitution of aluminum into the structure was

* Corresponding author. Current address: Jerry Barker Consultants, 10 Home Farm Close, Shipton-under-Wychwood, Oxfordshire OX7 6EH, United Kingdom.
E-mail address: jerrybarker@gmail.com (J. Barker).

0378-7753/$ – see front matter © 2007 Elsevier B.V. All rights reserved.
doi:10.1016/j.jpowsour.2007.06.079

achieved by preparing a $V_{1-x}Al_xPO_4$ intermediate. This material was prepared from V_2O_5 (Alfa-Aesar), $Al(OH)_3$ (Aldrich), $(NH_4)_2HPO_4$ (Alfa-Aesar) and high surface area carbon, all of which were intimately mixed using stoichiometric proportions and then pelletized. The precursor compositions were confirmed by ICP analysis. The second step was a simple LiF incorporation reaction. The precise preparative conditions have been described in detail elsewhere [5–7].

For electrochemical testing, composite electrodes were fabricated using 84 wt.% active material, 5 wt.% Super P (conductive carbon) and 11 wt.% PVdF-HFP co-polymer (Elf Atochem) binder. For all electrodes an aluminum current collector was employed. The electrolyte comprised a 1 M $LiPF_6$ solution in ethylene carbonate/dimethyl carbonate (2:1 w/w) while a dried glass fiber filter (Whatman, Grade GF/A) was used as electrode separator. High-resolution electrochemical measurements were performed using the electrochemical voltage spectroscopy (EVS) technique [12]. EVS is a voltage step method, which provides a high-resolution approximation to the open circuit voltage curve for the electrochemical system under investigation. Cycling tests were performed using a commercial battery cycler (Maccor Inc., Tulsa, OK, USA).

Structural and crystallographic analyses were based on X-ray powder diffraction data obtained using a Siemens D5000 diffractometer (in Bragg–Bretano geometry) equipped with Cu Kα radiation. Data was collected in the 2θ range of 10–50° using a step size of 0.02°. Structure refinement based on the Rietveld method was performed using the General Structure Analysis Software package (GSAS) of Larson and Von Dreele [13,14]. The analysis was performed in accordance with the method outlined by Young [15]. In this work we have assumed that the prepared materials all possess the amblygonite $LiAlPO_4F$ structure [9], and that the vanadium and aluminum atoms occupy the same crystallographic site within the structure.

3. Results and discussion

Fig. 1 depicts the raw XRD powder patterns obtained for the three experimental iterations. Other than the presence of some unreacted LiF, the $LiVPO_4F$ sample appears to be essentially phase pure. The two Al substituted samples, $LiV_{0.75}Al_{0.25}PO_4F$ and $LiV_{0.5}Al_{0.5}PO_4F$ have a low level of impurities present, which, after a detailed comparison with the ICDD PDF-2 database, were determined to be Li_3PO_4 and $AlPO_4$ [16,17]. The refined lattice parameters for the three experimental phases are summarized in Table 1, together with a comparison with the pure Al material, $LiAlPO_4F$. Close examination reveals that as the Al content is increased, the lattice parameters of the phases decrease smoothly. Linear regression analysis determined that the relationship between Al content and lattice parameters approximates to Vegard's Law, thus suggesting a full range solid solution between Al and V [18].

Results of the multiphase Rietveld analysis for $LiVPO_4F$ indicate that around 3% LiF is present as a second phase. This is unsurprising since the precursor VPO_4 contains 3.5% residual carbon, which was not corrected for in the LiF incorporation step. Further analysis on the $LiV_{0.75}Al_{0.25}PO_4F$ and

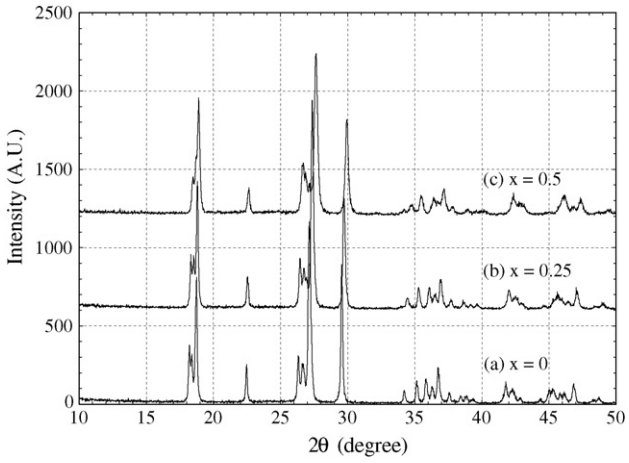

Fig. 1. XRD patterns for $LiV_{1-x}Al_xPO_4F$ phases with various Al contents: (a) $x=0$, (b) $x=0.25$ and (c) $x=0.5$. See text and Table 1 for the refined unit cell parameters.

$LiV_{0.50}Al_{0.50}PO_4F$ materials indicate the presence of both Li_3PO_4 and $AlPO_4$ as impurities at around the 1% level.

The structure of the $LiVPO_4F$ material is best described as tetrahedrally coordinated phosphate groups that corner share with octahedrally coordinated vanadium atoms. The vanadium/aluminum atoms are located on two crystallographically distinct sites, with each of the metals atoms bonded to four oxygen atoms and two fluorine atoms. The observed bond lengths for the PO_4 units range from 1.506(6) to 1.554(5) Å with an average bond length of 1.524(5) Å. Although theses values are within the range expected for this kind of material, comparison to the results of Beitone et al. for $LiGaPO_4F_{0.76}(OH)_{0.26}$ [9] and Simonov and Belov for $LiAlPO_4F$ [19] suggest that the PO_4 tetrahedra may be slightly distorted from a regular tetrahedra.

The electrochemical behavior (under constant current conditions) exhibited by the various aluminum-substituted lithium vanadium fluorophosphates, $LiV_{1-x}Al_xPO_4F$ is depicted in Fig. 2. The unsubstituted $LiVPO_4F$ ($x=0$) displays electrochemical behavior consistent with that described in our previous communications [6,7]. The constant current specific charge and discharge capacities obtained for this phase were 144 and 140 mAh g^{-1}, respectively, close to the theoretical material utilization of 155 mAh g^{-1}. The lithium extraction process in this region is characterized by a small inflection in the voltage curve, presumably reflecting sequential removal of lithium from the two energetically inequivalent sites within the $LiVPO_4F$ host framework. The average voltages for these two extraction processes correspond to the two charge plateaus at 4.25 and 4.29 V versus Li. The respective capacities for these two processes are 58 and 86 mAh g^{-1}. This represents an electrochemically predicted site occupancy ratio of 1:1.48. A single voltage plateau at around 4.2 V versus Li characterizes the subsequent lithium insertion reaction. The electrochemical behavior is more clearly represented in the differential capacity profiles (derived from EVS experiments), which are shown in Fig. 3. The upper EVS plot displays the pure $LiVPO_4F$ ($x=0$) phase. The two-site character of the charge profile is clearly defined. The single process

Table 1
Refined unit cell lattice parameters for $LiVPO_4F$, $LiV_{0.75}Al_{0.25}PO_4F$ and $LiV_{0.5}Al_{0.5}PO_4F$

	$LiVPO_4F$	$LiV_{0.75}Al_{0.25}PO_4F$	$LiV_{0.5}Al_{0.5}PO_4F$	$LiAlPO_4F$ Ref. [19]
a (Å)	5.167(9)	5.149(5)	5.127(3)	5.06
b (Å)	5.306(7)	5.275(9)	5.235(7)	5.16
c (Å)	7.290(0)	7.245(2)	7.192(6)	7.08
α (°)	108.91(7)	108.94(1)	108.89(7)	109.87
β (°)	107.22(7)	107.35(5)	107.59(6)	107.5
γ (°)	98.40(0)	98.55(3)	98.84(5)	97.9
Vol (Å^3)	174.0(4)	171.0(1)	167.2(2)	159.78

These results were derived from a Rietveld (GSAS) refinement of powder XRD data. For comparison, the lattice parameters for amblygonite, $LiAlPO_4F$ are also shown [19].

of the lithium insertion reaction is centered at 4.19 V versus Li.

The substitution of increasing levels of aluminum into the fluorophosphate structure yields some significant deviations in electrochemical behavior from that of the original $LiVPO_4F$ phase. With 25% substitution ($x = 0.25$) the charge and discharge capacities decrease to 117 and 112 mAh g^{-1}, respectively (Fig. 2). Again this compares favorably with the theoretical specific capacity of 121 mAh g^{-1}. This theoretical calculation is based on the assumptions that the aluminum is electrochemically inactive and that only the $V^{3+/4+}$ redox couple is operational.

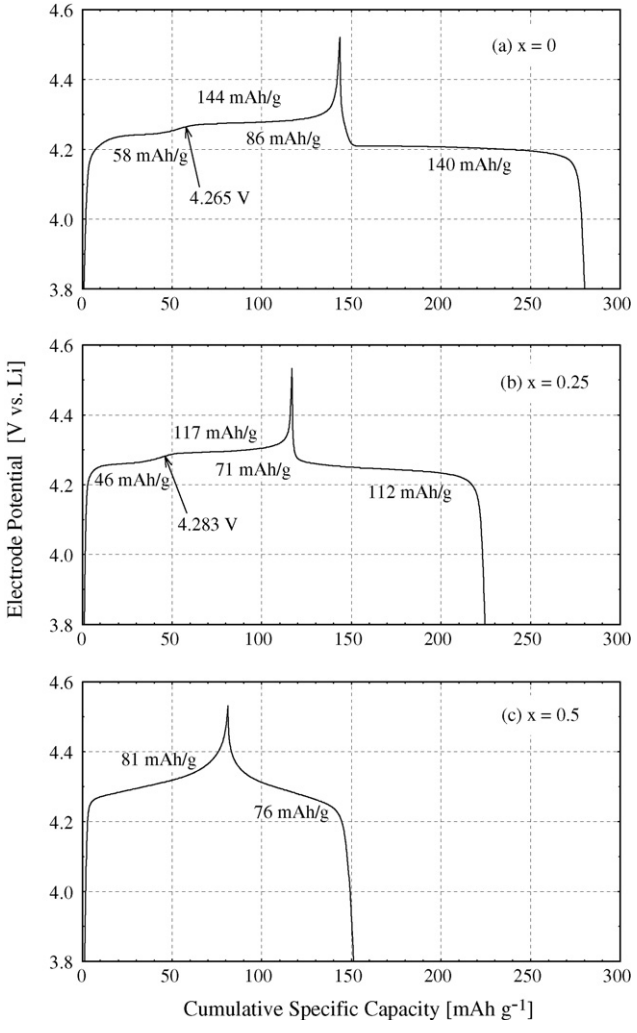

Fig. 2. Constant current electrochemical performance data for a range of cells with varying aluminum content according to the formula Li//$LiV_{1-x}Al_xPO_4F$. The cells were cycled between 3.00 and 4.50 V at approximately a *C*/5 rate for both charge and discharge. The data shown were collected at 23 °C and are for the first cycle. The electrolyte comprised a 1 M $LiPF_6$ solution in ethylene carbonate/dimethyl carbonate (2:1 w/w): (a) $x = 0$, (b) $x = 0.25$ and (c) $x = 0.5$. *Note*: the quoted specific capacity is based on 3.0–4.5 V.

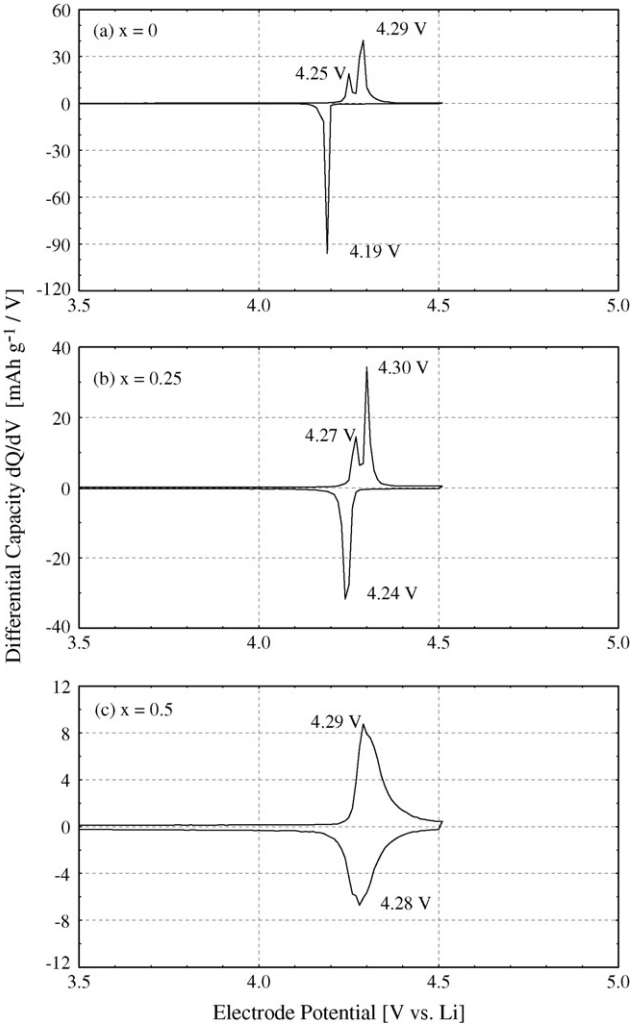

Fig. 3. EVS differential capacity data for a range of Li//$LiV_{1-x}Al_xPO_4F$ cells. The cells were cycled between 3.00 to 4.50 V at approximately a *C*/5 rate for both charge and discharge. The data shown were collected at 23 °C and are for the first cycle. The electrolyte comprised a 1 M $LiPF_6$ solution in ethylene carbonate/dimethyl carbonate (2:1 w/w): (a) $x = 0$, (b) $x = 0.25$ and (c) $x = 0.5$.

Clearly the two-plateau charge and one-plateau discharge behavior is retained. The average voltages for the two charge plateaus are 4.27 and 4.30 V versus Li (peak maxima taken from EVS data, Fig. 3). The corresponding specific capacities are 46 and 71 mAh g^{-1}, yielding a predicted site occupancy ratio of 1:1.54. On discharge, a single peak is observed at 4.24 V versus Li.

When the level of aluminum is increased to 50% ($x = 0.5$), the charge and discharge capacities are reduced further to 81 and 76 mAh g^{-1}, respectively. The theoretical capacity for this level of substitution (again based on a vanadium 3+/4+ transition) is 84 mAh g^{-1}. The overall voltage profile for this iteration, though, is markedly different. From the constant current plot (Fig. 2) the two-plateau nature of the lithium extraction process has disappeared and the plot now displays two single plateaus, one for charge and one for discharge. This is more clearly reflected in the differential capacity profiles (Fig. 3), which shows two, almost symmetrical peaks for charge and discharge centered at 4.29 and 4.28 V versus Li.

The incorporation of aluminum into the $LiVPO_4F$ structure has generated some interesting properties. First, the charge and discharge capacities on the V^{3+}/V^{4+} couple decrease almost linearly with aluminum substitution: varying from 144/140 to 117/112 to 81/76 mAh g^{-1}. This, in conjunction with the XRD data, reflects the smooth interchange between the aluminum and vanadium within the amblygonite-based structure. Second, the ratio of the two charge plateaus remains relatively constant for the $x = 0$ and 0.25 cases. This suggests that aluminum substitution does not affect significantly the Li site occupancy. This behavior may also pertain to the $x = 0.5$ case. Inspection of the differential capacity data (Fig. 3), reveals that there may not just be a single peak, but in fact, two peaks, but with significant overlap. Future work will involve carrying out further EVS studies at higher resolution (smaller voltage step intervals) in an attempt to resolve these additional features.

Third, the average charge and discharge voltages are increasing with increasing aluminum content. The first charge peak position shifts up in voltage to merge with the large peak, from 4.25 to 4.27 to 4.29 V versus Li. The second charge peak position appears to be insensitive to aluminum substitution and remains at 4.29–4.30 V versus Li. The discharge peak increased almost linearly from 4.19 to 4.24 to 4.28 V versus Li. Last, both the constant current and EVS plots show how the disorder in the system increases with higher aluminum content. In comparison with the initial pure $LiVPO_4F$, which was characterized by sharply defined peaks, the $LiV_{0.5}Al_{0.5}PO_4F$ phase appears much more diffuse. By contrast, the voltage hysteresis between lithium extraction and insertion decreases with increasing aluminum substitution, becoming almost negligible at just 0.01 V. This hints at the potential high rate and high-energy efficiency nature of the 50% doped material.

Within this study it was hoped that incorporation of Al into the $LiVPO_4F$ structure might activate the $V^{4+/5+}$ redox couple in these phases. Extensive experimentation on the $LiV_{0.75}Al_{0.25}PO_4F$ and $LiV_{0.5}Al_{0.5}PO_4F$ compositions using upper voltage limits as high as 5 V versus Li failed to reveal any significant electrochemical activity. It is possible that the $V^{4+/5+}$ redox transition is actually located at more positive potentials, but the tests described herein were limited by the stability window of the electrolyte.

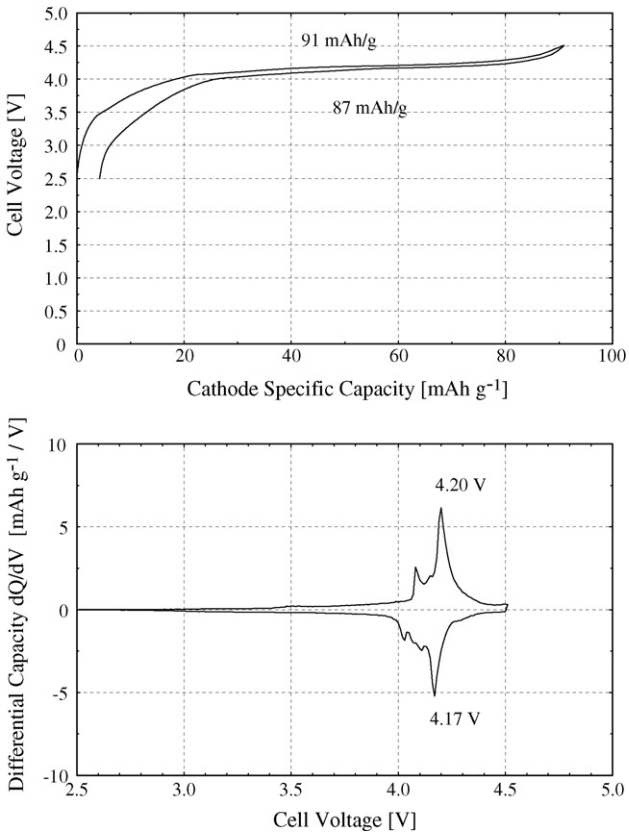

Fig. 4. EVS data for a typical graphite//$LiV_{0.5}Al_{0.5}PO_4F$ lithium-ion cell cycled between 2.50 and 4.50 V. The data shown were collected at 23 °C and are for the first cycle. The electrolyte comprised a 1 M $LiPF_6$ solution in ethylene carbonate/dimethyl carbonate (2:1 w/w): (top) EVS voltage profile; (bottom) EVS differential capacity profile.

Fig. 4 shows the EVS data for the $LiV_{0.5}Al_{0.5}PO_4F$ in a lithium-ion configuration using a crystalline graphite anode. First cycle capacities were 91 and 87 mAh g^{-1} for charge and discharge, respectively. The first cycle inefficiency is around the 5% for this test. In this configuration, the material still retains the low hysteresis and high symmetry shown in the half-cell configuration (versus lithium). The average discharge voltage for the lithium-ion configuration is high at 4.17 V. This compares favorably with the average discharge voltage of around 4.05 V for the unsubstituted $LiVPO_4F$ in a similar lithium-ion arrangement.

Fig. 5 demonstrates the preliminary life cycle performance for a larger range of the Al substituted $LiV_{1-x}Al_xPO_4F$ phases, where $x = 0$, 0.1, 0.25, and 0.5 in a graphite lithium-ion configuration. The initial specific capacity data, again, correlate well with the degree of substitution. Initial cycling ability also compares favorably across the entire compositional range. With the possible exception of the $x = 0.1$ iteration, these preliminary findings suggest that the modified phases will cycle at least as well as the pure $LiVPO_4F$.

In Fig. 6 the cycling behavior of the graphite// $LiV_{0.9}Al_{0.1}PO_4F$ lithium-ion system is demonstrated as a function of rate, using three different charge/discharge regimens. Under all experimental conditions (*C*/7, *C*/2 and *C* rates)

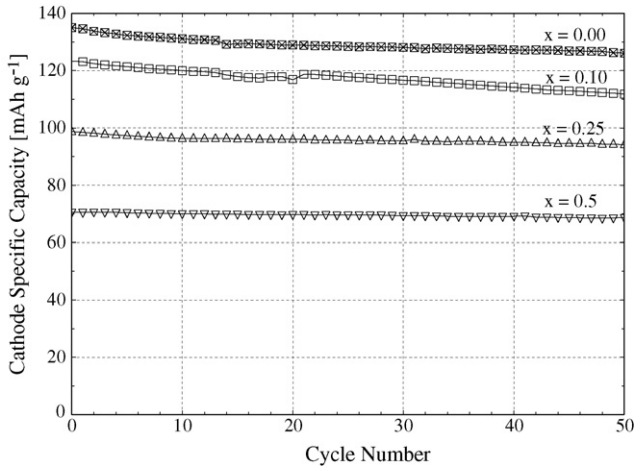

Fig. 5. Preliminary cycling data for a range of graphite// $LiV_{1-x}Al_xPO_4F$ lithium-ion cells. The cells were cycled between 3.00 and 4.40 V at an approximate *C*/7 rate for both charge and discharge. The data shown were collected at 23 °C. The electrolyte comprised a 1 M $LiPF_6$ solution in ethylene carbonate/dimethyl carbonate (2:1 w/w): (a) $x = 0$, (b) $x = 0.1$, (c) $x = 0.25$ and (d) $x = 0.5$.

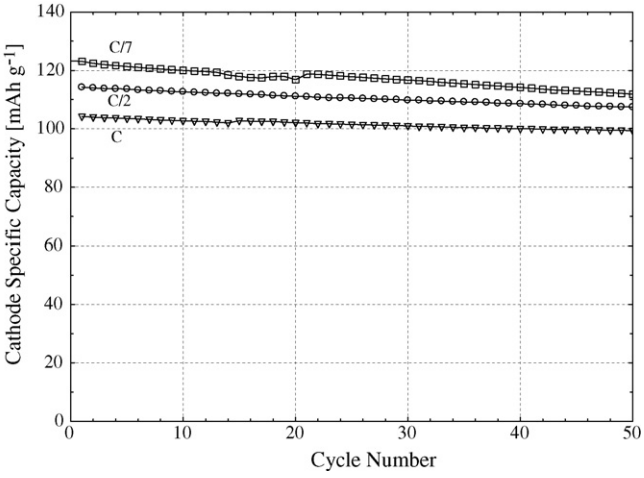

Fig. 6. Comparative cycling behavior of graphite// $LiV_{0.9}Al_{0.1}PO_4F$ lithium-ion cells cycled at different charge/discharge rates (as indicated). The cells were cycled between 3.00 and 4.40 V and the data shown were collected at 23 °C. The electrolyte comprised a 1 M $LiPF_6$ solution in ethylene carbonate/dimethyl carbonate (2:1 w/w).

the system shows encouraging initial performance. As expected the material specific capacity for the cathode decreases on increasing the cycling rate.

4. Conclusions

The results presented in this study reflect the versatile nature of the lithium vanadium fluorophosphate, $LiVPO_4F$ phase with respect to aluminum substitution. The aluminum appears to exchange smoothly with vanadium according to the general composition $LiV_{1-x}Al_xPO_4F$, to generate a range of novel electroactive phases. XRD data show that the basic triclinic amblygonite structure was retained for all the substituted materials that were considered, up to a 50% aluminum content. In lithium metal test cells the material specific capacities decreased almost linearly with aluminum exchange. Under our current electrochemical testing conditions we were unable to activate the $V^{4+/5+}$ redox couple, with access being restricted to the $V^{3+/4+}$ couple. Despite this limitation, the doped phases revealed some intriguing properties that appear to be 'tunable' within the compositional range under investigation. In a lithium-ion configuration several attractive attributes were also established, including low voltage polarization, high operating voltage, low charge irreversibility and good (predicted) life cycle.

References

[1] A.K. Padhi, K.S. Nanjundaswamy, C. Masquelier, J.B. Goodenough, J. Electrochem. Soc. 144 (1997) 2581.
[2] (a) J. Barker, M.Y. Saidi, US Patent 5,871,866 (filed September 1996, issued February 1999);
(b) M.Y. Saidi, J. Barker, H. Huang, J.L. Swoyer, G. Adamson, Electrochem. Solid State Lett. 5 (2002) A149.
[3] J. Barker, M.Y. Saidi, J. Swoyer, US Patent 6,387,568 (filed April 2000, issued May 2002).
[4] J. Barker, M.Y. Saidi, J. Swoyer, J. Electrochem. Soc. 150 (2003) A1394.
[5] J. Barker, M.Y. Saidi, J. Swoyer, J. Electrochem. Soc. 151 (2004) A1670.
[6] J. Barker, R.K.B. Gover, P. Burns, A. Bryan, M.Y. Saidi, J. Swoyer, J. Power Sources 146 (2005) 516.
[7] J. Barker, R.K.B. Gover, P. Burns, A. Bryan, M.Y. Saidi, J.L. Swoyer, Proceedings of the International Meeting on Lithium Batteries, Abstract 285, Nara, Japan, June 27–July 2, 2004.
[8] (a) Th. Loiseau, Y. Calage, P. Lacorre, G. Ferey, J. Solid State Chem. 111 (1994) 390;
(b) L.A. Groat, B.C. Chakoumakos, D.H. Brouwer, C.M. Hoffman, C.A. Fyfe, H. Morell, A.J. Schultz, Am. Mineral. 88 (2003) 195;
(c) L.A. Groat, M. Raudsepp, F.C. Hawthorne, T.S. Ercit, B.L. Sheriff, Am. Mineral. 75 (1990) 992.
[9] (a) A.A. Moss, E.E. Fejer, P.G. Embrey, Mineral. Mag. 37 (1969) 414;
(b) L. Beitone, N. Guillou, F. Millang, Th. Loiseau, G. Ferey, Solid State Sci. 4 (2002) 1061.
[10] H.T. Ellingham, J. Soc. Chem. Ind. 63 (1944) 125.
[11] J.D. Gilchrist, Extraction Metallurgy, 2nd ed., Pergamon Press, Oxford, 1980, p. 161.
[12] J. Barker, Electrochim. Acta 40 (1995) 1603.
[13] H.M. Rietveld, J. Appl. Crystallogr. 2 (1969) 65.
[14] A.C. Larsen, R.B. Von Dreele, Los Alamos Laboratory Report NO-LA-U-86-746, 1987.
[15] R.A. Young, The Rietveld Method, Oxford Science Publications (Chapter 1), 1993.
[16] C. Keffer, A.D. Mighell, F. Mauer, H. Swanson, S. Block, Inorg. Chem. 6 (1967) 119–125.
[17] J.W. Richardson Jr., J.J. Pluth, J.V. Smith, Acta Crystallogr. B 44 (1988) 367–373.
[18] L. Vegard, Z. Phys. 5 (1921) 17;
M.F. Thorpe, E.J. Garboczi, Phys. Rev. B 42 (1990) 8405–8414.
[19] W.I. Simonov, N.V. Belov, Kristallografiya 3 (1958) 428.